RESEARCH ARTICLE | SEPTEMBER 02 2015

Generation of localized strain in a thin film piezoelectric to control individual magnetoelectric heterostructures

Jizhai Cui; Cheng-Yen Liang; Elizabeth A. Paisley; Abdon Sepulveda ; Jon F. Ihlefeld; Gregory P. Carman; Christopher S. Lynch

Appl. Phys. Lett. 107, 092903 (2015)
https://doi.org/10.1063/1.4930071
CHORUS

Generation of localized strain in a thin film piezoelectric to control individual magnetoelectric heterostructures

Jizhai Cui,[1] Cheng-Yen Liang,[1] Elizabeth A. Paisley,[2] Abdon Sepulveda,[1] Jon F. Ihlefeld,[2] Gregory P. Carman,[1] and Christopher S. Lynch[1,a)]
[1]*Department of Mechanical and Aerospace Engineering, University of California, Los Angeles, California 90095, USA*
[2]*Electronic, Optical, and Nano Materials Department, Sandia National Laboratories, Albuquerque, New Mexico 87185, USA*

(Received 31 March 2015; accepted 23 August 2015; published online 2 September 2015)

Experimental results demonstrate the ability of a surface electrode pattern to produce sufficient in-plane strain in a $PbZr_{0.52}Ti_{0.48}O_3$ (PZT) thin film clamped by a Si substrate to control magnetism in a 1000 nm diameter Ni ring. The electrode pattern and the Ni ring/PZT thin film heterostructure were designed using a finite element based micromagnetics code. The magnetoelectric heterostructures were fabricated on the PZT film using e-beam lithography and characterized using magnetic force microscopy. Application of voltage to the electrodes moved one of the "onion" state domain walls. This method enables the development of complex architectures incorporating strain-mediated multiferroic devices. © *2015 AIP Publishing LLC*.
[http://dx.doi.org/10.1063/1.4930071]

Manipulating magnetization at the micro- and nanoscale has been studied extensively for next-generation computer memory, nanoscale sensors, and spintronic devices.[1,2] Magnetization can be controlled by magnetic field,[3] spin-polarized current injection,[4] exchange-bias,[5,6] interface-charge-driven magnetoelectric (ME) effect,[7,8] strain-mediated ME effect,[9–11] and ferroelectric/ferromagnetic coupling in single phase multiferroics.[6] The use of strain-mediated approach to control magnetization is attracting increasing attention due to its promising low energy consumption, large coupling coefficient, and the wide availability of piezoelectric/magnetoelastic materials.[10,12] Previous research has demonstrated magnetization manipulation of nanoscale ellipses,[11] squares,[13] and ring[14] structures using bulk piezoelectric substrates. Bulk piezoelectric substrates switch all elements at once,[11] require high voltage, are semiconductor incompatible and are rate limited by elastic wave velocities through the thickness; all of these challenges must be overcome for magnetoelectric device design.

Compared to bulk piezoelectrics, piezoelectric thin films require much smaller voltage to obtain similar magnitude of electric field ($E = V/d$, where V and d refer to applied voltage and thickness of piezoelectrics, respectively). The thickness mode response time becomes shorter as the thickness is decreased ($\tau = d/c$, where d is the film thickness and c is the bulk acoustic wave velocity; for a 1 μm thick film with $c = 4000$ m/s, the thickness mode response time is on the order of 0.25 ns). Thin film piezoelectrics have much smaller device volume, reducing the energy required to drive the combination of piezoelectric strain and magnetization reorientation needed for nanoarchitected magnetoelectric devices. Furthermore, piezoelectric films are used in a range of MEMS devices.[15,16] Few researchers have reported using thin film piezoelectrics to alter magnetization of nanoscale magnetic elements. Chung *et al.*[17] reported magnetic domain evolution using a fully electroded lead zirconate titanate (PZT) thin film when voltage was applied. However, this approach did not offer the ability to control individual nano-architected magnetoelectric elements. To date, this capability has been lacking.

Achieving local control of individual magnetoelectric structures on a piezoelectric thin film is a challenging problem. Piezoelectric thin films are fully clamped in-plane by the substrate. This dramatically reduces the effective piezoelectric coefficient[18] and hence restricts its capability of generating enough strain for controlling magnetization. To reduce the clamping effect, researchers reported etching PZT film into discrete islands.[19,20] However, this complicated fabrication process may limit its applications. We present a concept using electrode pattern design to control in-plane magnetoelastic anisotropy by creating a highly localized strain at the surface of a piezoelectric thin film subject to substrate clamping. Finite element simulations (FEA) were used to design the electrode pattern and the magnetic element. These devices were fabricated and the magnetic domain pattern in the Ni ring was shown to change in response to the induced localized strain.

A conceptual schematic of the technique is presented in Figure 1(a), derived from previous research by Cui *et al.*[21] The structure consists of a Si wafer substrate (not shown), a bottom electrode, a PZT thin film, and, in this case, three pairs of electrodes surrounding a middle magnetic element. When voltage is applied to one pair of top electrodes (A-A, B-B, or C-C) while the bottom electrode is grounded, the piezoelectric material underneath each electrode expands out-of-plane (d_{33} effect) and contracts in-plane (d_{31} effect), creating a highly localized strain field under each electrode and in their immediate vicinity. When two such electrodes

a)Author to whom correspondence should be addressed. Electronic mail: cslynch@seas.ucla.edu

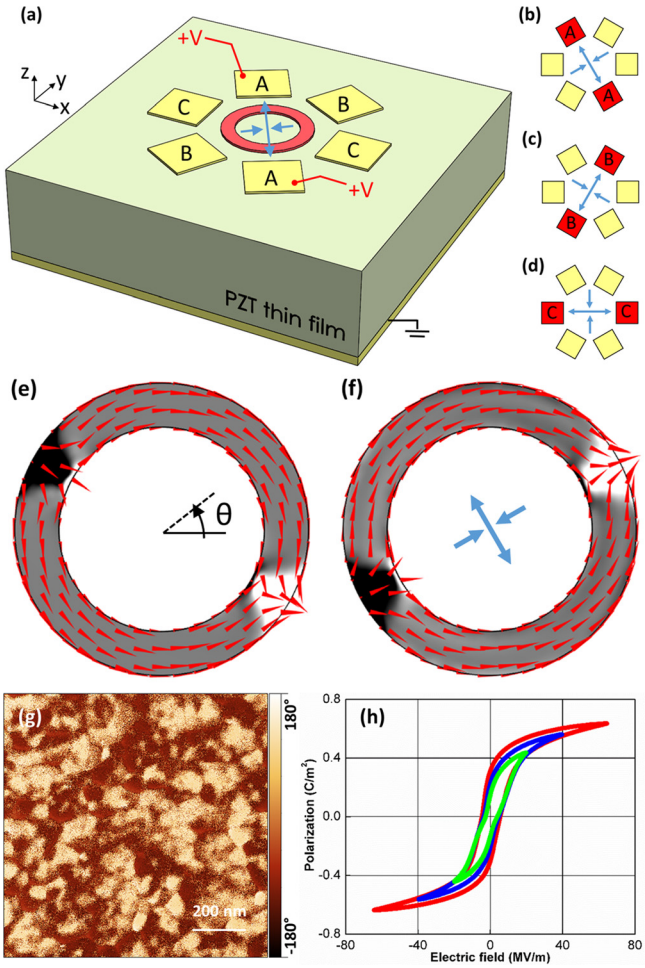

FIG. 1. (a) Schematic of a device structure that can create magnetoelastic anisotropy on magnetic elements (a ring is shown as an example) in three directions by applying voltage on (b)–(d) A-A, B-B, or C-C electrodes. Blue arrows illustrate the average principal strain direction between electrodes for each case with the outward pointing arrows indicating the tensile strain and inward pointing arrows indicating the compressive strain directions. (e) Results of a micromagnetic simulation of a 1000 nm outer diameter, 700 nm inner diameter, and 15 nm thick Ni ring initialized along $\theta = -30°$ direction by an applied magnetic field. The red arrows indicate the local in-plane magnetization direction. Grayscale color indicates the local out-of-plane magnetization. (f) Results of a micromagnetic simulation of a Ni ring subject to a 1200 ppm biaxial strain with the tensile and compression direction indicated by blue arrows. (g) A piezoelectric force microscopy (PFM) phase image of the PZT thin film. (h) A polarization versus electric field (P-E) loop of the PZT thin film.

are in close proximity, the strain fields surrounding the electrodes interact and an in-plane bi-axial strain field is induced between the electrodes (tensile along the axis connecting the electrodes and compressive in the orthogonal direction). Figures 1(b)–1(d) show the average principal strain field between electrodes when voltage is applied to the A-A, B-B, and C-C electrodes, respectively. Considering Ni as an example (negative magnetostriction), this principal strain field induces magnetoelastic anisotropy with the easy axis aligned with the compressive strain direction.[3] Hence, in the conditions shown in Figure 1(b)–1(d), three different in-plane magnetoelastic anisotropy directions can be achieved by applying voltage to each of the three different pairs of electrodes (A-A, B-B, or C-C). In this ideal case, the three pairs of electrodes spaced 60° apart are sufficient to deterministically manipulate magnetization of magnetic elements.

The magnitude of the induced bi-axial strain in the structure when voltage is applied was approximated using linear piezoelectric FEA simulations.[21] The piezoelectric coefficients and dimensions used in the simulations were $d_{33} = 70$ pC/N, electrode dimension $0.6 \times 0.6\ \mu m^2$, electrode separation distance 1.4 μm, PZT thin film thickness 1.0 μm, and applied voltage 25 V. In the simulation, the bottom surface of the PZT thin film was fixed to simulate the clamped substrate boundary condition. The simulations (results not shown) indicated that approximately 1200 ppm average biaxial strain (principal strain $\varepsilon_x - \varepsilon_y > 0$) can be generated between the electrodes. A micromagnetic model[22] based on the Landau-Lifshitz-Gilbert (LLG) equation including magnetoelastic coupling implemented in a finite element framework was used to design Ni ring elements with a domain structure that responds to this level of strain. Figure 1(e) shows the simulation results for a Ni ring with 1000 nm outer diameter, 700 nm inner diameter, and 15 nm thickness. In the simulations, the Ni ring of this geometry formed the "onion" state[23] when magnetization was initialized at $\theta = -30°$ direction. The black and white regions on the ring are the position of two 180° head-to-head domain walls where there is an out-of-plane magnetization component. When the 1200 ppm biaxial strain was applied in the $\theta = 30°$ direction (the direction of biaxial strain is defined by the direction of the compressive strain), the ring magnetization rotated counterclockwise by 60° and aligned with the compressive strain direction. When strain was unloaded, the magnetization stayed at the new position ($\theta = 30°$). Hence, if the Ni ring is initialized along $\theta = -30°$ direction, the application of 25 V to the A-A electrodes generates strain that rotates the magnetization from $\theta = -30°$ to $\theta = 30°$. Similarly, starting from the magnetization along $\theta = +30°$ and applying 25 V to the C-C electrodes as shown in Figure 1(d), the simulation results indicate that the magnetization should rotate to the $\theta = +90°$ direction (along the compressive strain). Starting from the magnetization along $\theta = +30°$ and applying 25 V to the B-B electrodes as shown in Figure 1(c), simulation results indicate that the magnetization rotated back to the $\theta = -30°$ direction. Hence, it is possible to deterministically control the magnetization direction of the "onion" domain state in a 1000 nm diameter Ni ring.

The resulting design was fabricated on a chemical solution deposited 1 μm thick $PbZr_{0.52}Ti_{0.48}O_3$ film on 100 nm Pt (bottom electrode)/40 nm ZnO/400 nm SiO_2/Si substrate. Details of the preparation process of this film are given in a previous publication.[24] The piezoelectric force microscopy (PFM) image in Figure 1(g) shows a clear piezoelectric response, highlighting out-of-plane piezoelectric phase. An effective piezoelectric constant of the film of $d_{33,e} = 49.2$ pC/N was measured by PFM. Because $d_{33,e}$ is measured on a clamped film, it is lower than the actual piezoelectric constant d_{33} of the film.[18,25] Hence in the piezoelectric FEA simulations, the stress free piezoelectric constant was estimated to be $d_{33} = 70$ pC/N (about 40% higher than $d_{33,e}$). The root-mean-squared surface roughness of the film was $R_q = 1.35$ nm. The polarization versus electric field (P-E) hysteresis loop in Figure 1(h) shows that the electrical coercive field is about 5 MV/m. The electric breakdown value of the film is about 70 MV/m. The electrode patterns and

magnetic Ni ring structure were defined using a two-step e-beam lithography process. Electrodes of 5 nm Ti and 100 nm Au were deposited by e-beam evaporation. By the same technique, 3 nm Ti and 15 nm Ni were deposited, followed by 2 nm Al as a capping layer protecting the Ni from oxidation. The size of the electrodes, electrode separation distance, and Ni ring geometry were identical to the parameters used in the FEA simulation.

Figure 2(a) is an atomic force microscopy (AFM) image of the fabricated device showing the Ni ring structure and three pairs of electrodes on the PZT thin film. Magnetic force microscopy (MFM) was used to determine the magnetization configuration of the Ni ring structure. It is challenging to image soft magnetic material (such as Ni) elements under MFM due to the tip stray field.[26] However, several previous studies have acquired MFM images on Ni micro- and nanostructures by carefully choosing tip coating, operation mode, and parameters.[14,27] A low moment tip (MESP-LM, Bruker) was used and the tip lift height during the measurement was 40 nm. At least two images were recorded in the same condition with different scanning directions. When there was a clear difference between them (which came from undesired tip-sample interaction), the images were discarded. Figures 2(a) and 2(c) show AFM and MFM images of the as-fabricated device. The nickel ring displays the PZT surface roughness, i.e., humps and grooves of the PZT grain structure, as seen in Figure 2(b). As MFM measures the magnitude of out-of-plane magnetization, the "onion" state of the Ni ring can be identified as black and white spots in the MFM image as shown in Figure 2(c). 25 V was then applied to the B-B electrodes and held for 20 s. After unloading the voltage, the MFM measurement was again conducted and the result is shown in Figure 2(d).

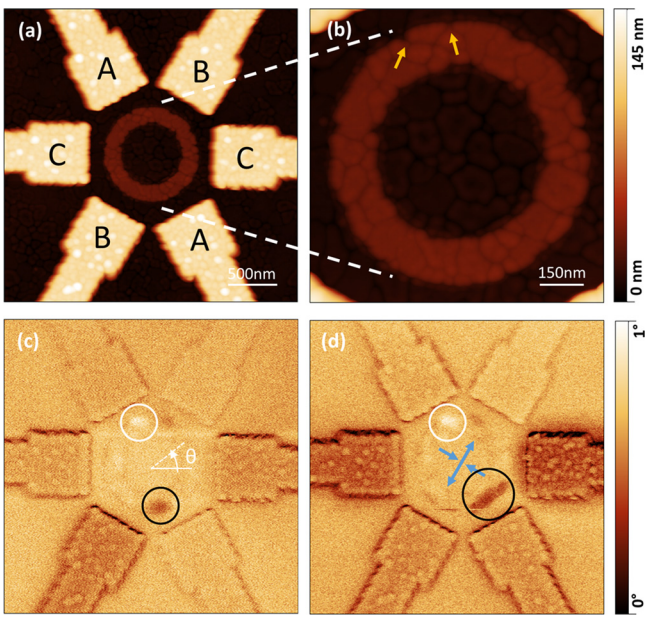

FIG. 2. (a) An AFM picture of the fabricated device with a Ni ring surrounded by patterned electrodes; (b) expanded view of the Ni ring. The yellow arrows indicate the position of two observed notches. (c) An MFM image of the as-fabricated device initialized by an applied magnetic field with two "onion" state domain walls shown as black and white spots (circled); (d) after applying 25 V to the B-B electrodes one magnetic domain has moved and spread (black circle). The blue arrows indicate the direction of average principal strain induced by the applied voltage.

The results show that the patterned electrode approach produces sufficient in-plane strain to interact with the magnetization. In MFM images, some electrodes are darker than others. This is possibly due to accumulated charge sensed by the MFM tip through electrostatic force. This does not affect the magnetization measurement. There is a change of the domain wall structure seen by comparing Figures 2(c) and 2(d). The white spot mostly stayed unchanged, while the black spot was broadened. The broadening direction agreed with the direction of compressive strain (and hence the easy axis of magnetoelastic anisotropy). The arrows in Figure 2(b) indicate two notches that are physically on each side of the "white" magnetic domain wall. The two notches could be creating a deep energy well that pins the magnetic domains.[28] The observed domain wall broadening (black spot) could be due to the same mechanism; however, the local spins further from the notch become aligned with the magnetoelastic anisotropy. Hence, the combination of geometric imperfection and applied strain creates an overall effect of broadening the black magnetic domain wall.

Figure 3(a) shows the as-fabricated AFM images of a second fabricated device. The black and white spots in the MFM image are not perfectly symmetric, suggesting the magnetic domain walls might be trapped in local energy wells associated with geometric imperfections. Figure 3(b) shows the surface profiles of a Ni ring structure (profiles 1 and 3) and PZT thin film (profiles 2 and 4). Surface profiles for both Ni and PZT have about 6 nm peak-to-peak variation, showing that the Ni layer carried the topography from the PZT layer, which may affect the in-plane magnetization and induce magnetic domain wall pinning. Figure 3(c) is the MFM image of the as-fabricated device. 25 V was applied to electrode pair A-A and held for 20 s. After unloading the voltage, the MFM image shown in Figure 3(d) was taken. The white domain wall (highlighted in the dashed circle) shows a counterclockwise rotation from $\theta \approx -30^\circ$ to $\theta \approx 0^\circ$, while the black domain wall displays no significant motion. We note that in concept the white domain should align with the compressive strain direction at $\theta \approx 30^\circ$ direction, yet does not move that far. The reduced rotation is attributed to a notch seen at $\theta \approx 0^\circ$ in the AFM image (see arrows in Figure 3(a)). We then applied 25 V to the B-B electrodes and kept the voltage on for 20 s. Upon removal of the voltage, the MFM image was taken and shown in Figure 3(e). The white domain wall rotated clockwise back to $\theta \approx -30^\circ$ aligned with the compressive strain direction. As seen in Figures 3(c)–3(e), the magnetic domain structure of a Ni ring was rotated forward and backward using patterned electrodes on a fully clamped PZT thin film.

The observations above indicate that the domain walls become pinned by edge imperfections in the ring structure. These imperfections were the result of interaction of the lithography with the surface roughness of the columnar grain structured PZT thin film. Finite element based micromagnetic simulations were run to explore the interaction between the notches and a ring's domain structures. The notch was represented by a semi-ellipse with 50 nm major and 30 nm minor axes. This is about the size of the notch observed in

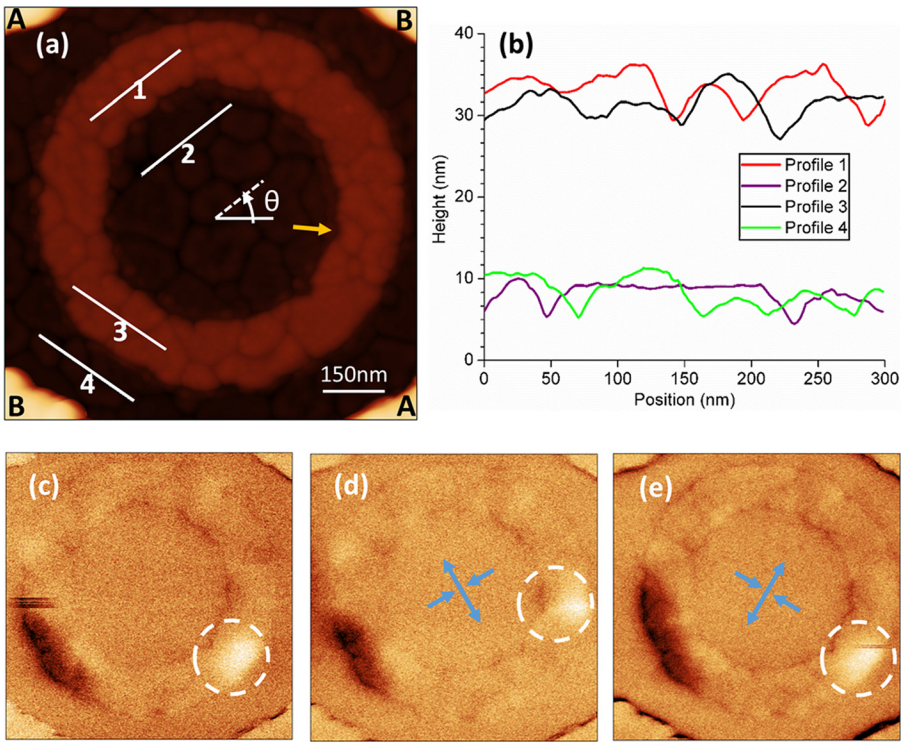

FIG. 3. (a) An AFM image of the second fabricated device. The yellow arrow indicates the position of an observed notch. (b) The height of the profiles corresponding to the four lines shown in (a). Note that the lines on the Ni ring are offset by the Ni thickness. (c) An MFM image of the as-fabricated Ni ring; (d) one domain wall (circled) has moved after applying 25 V to the A-A electrodes; (e) the same domain wall (circled) has moved back to its original position after applying 25 V to the B-B electrodes. The blue arrows indicate the direction of average principal strain induced by the applied voltage.

Figure 3(a). Figure 4(a) shows the geometry simulated with the notch on the inner diameter circled. When initialized along the $\theta = -30°$ direction, the Ni ring formed the "onion" state domain structure as shown (two 180° domain walls). 1200 ppm biaxial strain with compressive strain along $\theta = 30°$ direction was applied as illustrated by the blue arrows in Figure 4(b). The black domain wall rotated clockwise by 60° and aligned with the compression direction, but the white domain wall stopped at the $\theta = 0°$ direction, pinned by the notch. The simulation shows that the existence of the geometrical notch creates a local magnetic energy minimum that can pin the domain wall.

Two examples were presented from a large array of devices that were fabricated, all with same electrode pattern and Ni ring structure. In all cases, the patterned electrodes on the clamped PZT film produced sufficient strain to change the magnetic domain pattern. The domain wall structures

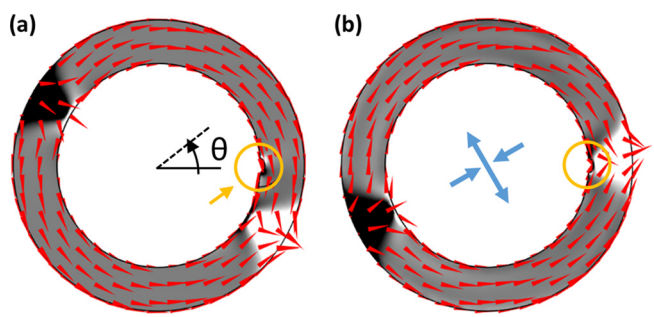

FIG. 4. The results of a micromagnetic simulation of a 1000 nm outer-diameter, 700 nm inner-diameter, and 15 nm thick Ni ring with a notch (semi-ellipse with 50 nm long axis and 30 nm short axis) at $\theta = 0°$ position. The magnetization distribution is shown (a) when initialized along $\theta = -30°$ direction and (b) after applying 1200 ppm bi-axial strain with the strain direction shown as blue arrows. The magnetic domain wall (white spot) has been pinned by the notch. The red arrows indicate the in-plane magnetization direction. Grayscale color indicates the out-of-plane magnetization.

changed by the strain field are the result of minimization of the magnetoelastic anisotropy and the shape anisotropy contributions to the free energy.[3] In most cases, only one magnetic domain wall (white or black spot in MFM image) moved in response to the applied voltage. Due to magnetic domain pinning, we were not able to achieve continuous 180° magnetization rotation by applying a voltage on A-A, B-B, and C-C, consecutively. In an attempt to reduce the surface topography effect, 25 nm thick Ni rings were produced with exact same geometry (1000 nm outer-diameter and 700 nm inner-diameter) on the same batch of PZT film. In the 25 nm thick Ni devices, similar magnetic domain rotation was observed after voltage was applied and the pinning effect did not appear to be reduced. This suggests that the edge imperfections may be contributing more to the pinning than the surface roughness. The PZT topography is mostly from grain boundary grooving, which is intrinsic for sol-gel prepared films. Possible methods to smooth the film surface include liquid phase coatings that are smoothed by surface tension, or pulsed layer deposition (PLD) prepared epitaxial PZT films.

In this paper, it was demonstrated that the use of patterned electrodes can overcome the clamping effect of the substrate in PZT films grown on Si. The resulting in-plane strain was demonstrated to be sufficiently large to interact with the magnetization of Ni rings. The elements were designed using a finite element based micromagnetics code. Geometric imperfections arising from the PZT surface topography were observed to interact with the domain wall motion and pin the domain walls. The patterned approach is applicable to many nanoscale strain-mediated magnetoelectric devices. The electrodes can be in different shapes as long as one of the dimensions is comparable to the film thickness. The magnetic structures can be placed on top of square electrodes to obtain bi-axial compressive strain, on

top of line electrodes to obtain uniaxial compressive strain, or between two line electrodes to obtain uniaxial tensile strain. The electrodes themselves can even be the magnetic material. This capability opens a design space for nanoarchitected magnetoelectric devices.

The authors would like to thank Dr. Scott Keller and Paul Nordeen for valuable discussions. This work was supported by NSF Nanosystems Engineering Research Center for Translational Applications of Nanoscale Multiferroic Systems (TANMS) Cooperative Agreement Award (No. EEC-1160504). Sandia National Laboratories is a multi-program laboratory managed and operated by Sandia Corporation, a wholly owned subsidiary of Lockheed Martin Corporation, for the U.S. Department of Energy's National Nuclear Security Administration under Contract No. DE-AC04-94AL85000.

[1]S. A. Wolf, D. D. Awschalom, R. A. Buhrman, J. M. Daughton, S. von Molnár, M. L. Roukes, A. Y. Chtchelkanova, and D. M. Treger, Science **294**, 1488 (2001).
[2]S. S. P. Parkin, M. Hayashi, and L. Thomas, Science **320**, 190 (2008).
[3]R. C. O'handley, *Modern Magnetic Materials: Principles and Applications* (Wiley, New York, 2000).
[4]J.-E. Wegrowe, D. Kelly, P. Guittienne, and J.-P. Ansermet, Europhys. Lett. **56**, 748 (2001).
[5]P. Borisov, A. Hochstrat, X. Chen, W. Kleemann, and C. Binek, Phys. Rev. Lett. **94**, 117203 (2005).
[6]Y.-H. Chu, L. W. Martin, M. B. Holcomb, M. Gajek, S.-J. Han, Q. He, N. Balke, C.-H. Yang, D. Lee, W. Hu, Q. Zhan, P.-L. Yang, A. Fraile-Rodríguez, A. Scholl, S. X. Wang, and R. Ramesh, Nat. Mater. **7**, 478 (2008).
[7]H. J. A. Molegraaf, J. Hoffman, C. A. F. Vaz, S. Gariglio, D. Van Der Morel, C. H. Ahn, and J. M. Triscone, Adv. Mater. **21**, 3470 (2009).
[8]C. A. F. Vaz, J. Hoffman, Y. Segal, J. W. Reiner, R. D. Grober, Z. Zhang, C. H. Ahn, and F. J. Walker, Phys. Rev. Lett. **104**, 127202 (2010).
[9]T. Wu, A. Bur, P. Zhao, K. P. Mohanchandra, K. Wong, K. L. Wang, C. S. Lynch, and G. P. Carman, Appl. Phys. Lett. **98**, 012504 (2011).
[10]J.-M. Hu, Z. Li, L.-Q. Chen, and C.-W. Nan, Nat. Commun. **2**, 553 (2011).
[11]M. Buzzi, R. V. Chopdekar, J. L. Hockel, A. Bur, T. Wu, N. Pilet, P. Warnicke, G. P. Carman, L. J. Heyderman, and F. Nolting, Phys. Rev. Lett. **111**, 027204 (2013).
[12]C. W. Nan, M. I. Bichurin, S. Dong, D. Viehland, and G. Srinivasan, J. Appl. Phys. **103**, 031101 (2008).
[13]S. Finizio, M. Foerster, M. Buzzi, B. Krüger, M. Jourdan, C. A. F. Vaz, J. Hockel, T. Miyawaki, A. Tkach, S. Valencia, F. Kronast, G. P. Carman, F. Nolting, and M. Kläui, Phys. Rev. Appl. **1**, 021001 (2014).
[14]J. L. Hockel, A. Bur, T. Wu, K. P. Wetzlar, and G. P. Carman, Appl. Phys. Lett. **100**, 022401 (2012).
[15]S. Trolier-McKinstry and P. Muralt, J. Electroceramics **12**, 7 (2004).
[16]S. Tadigadapa and K. Mateti, Meas. Sci. Technol. **20**, 092001 (2009).
[17]T.-K. Chung, S. Keller, and G. P. Carman, Appl. Phys. Lett. **94**, 132501 (2009).
[18]R. N. Torah, S. P. Beeby, and N. M. White, J. Phys. D: Appl. Phys. **37**, 1074 (2004).
[19]V. Nagarajan, A. Roytburd, A. Stanishevsky, S. Prasertchoung, T. Zhao, L. Chen, J. Melngailis, O. Auciello, and R. Ramesh, Nat. Mater. **2**, 43 (2003).
[20]V. Nagarajan, Appl. Phys. Lett. **87**, 242905 (2005).
[21]J. Cui, J. L. Hockel, P. K. Nordeen, D. M. Pisani, C. Liang, G. P. Carman, and C. S. Lynch, Appl. Phys. Lett. **103**, 232905 (2013).
[22]C.-Y. Liang, S. M. Keller, A. E. Sepulveda, A. Bur, W.-Y. Sun, K. Wetzlar, and G. P. Carman, Nanotechnology **25**, 435701 (2014).
[23]M. Kläui, C. A. F. Vaz, L. Lopez-Diaz, and J. A. C. Bland, J. Phys.: Condens. Matter **15**, R985 (2003).
[24]C. T. Shelton, P. G. Kotula, G. L. Brennecka, P. G. Lam, K. E. Meyer, J.-P. Maria, B. J. Gibbons, and J. F. Ihlefeld, Adv. Funct. Mater. **22**, 2295 (2012).
[25]R. Steinhausen, T. Hauke, W. Seifert, V. Mueller, H. Beige, S. Seifert, and P. Lobmann, in *Proceedings of 11th IEEE International Symposium on Applications of Ferroelectrics 98* (Piscataway, NJ, 1998), p. 93.
[26]X. Zhu, P. Grütter, V. Metlushko, and B. Ilic, J. Appl. Phys. **91**, 7340 (2002).
[27]X. Zhu, P. Grütter, V. Metlushko, and B. Ilic, J. Appl. Phys. **93**, 7059 (2003).
[28]M. Kläui, J. Phys.: Condens. Matter **20**, 313001 (2008).